Chemical Physics Letters 739 (2020) 136979

Contents lists available at ScienceDirect

Chemical Physics Letters

journal homepage: www.elsevier.com/locate/cplett

Research paper

Polymerization of aluminate monomer in its initial nucleation stage of organic alkali solution revealed by ReaxFF molecular dynamics simulation

Jianwei Guo[a,b], Shuangyi Liu[a], Zhi Wang[a,b,*], Jianwei Cao[a], Dong Wang[a]

[a] Key Laboratory of Green Process and Engineering, National Engineering Laboratory for Hydrometallurgical Cleaner Production Technology, Institute of Process Engineering, Chinese Academy of Sciences, Beijing 100190, PR China
[b] University of Chinese Academy of Sciences, Beijing 100039, PR China

HIGHLIGHTS

- Moderate organic alkali medium was designed to capture aluminate species.
- The $TMAH^+$ cation acts as bridge in the process of aluminate evolution.
- $TMAH^+$ cation promotes the transformation from monomer to polymeric multimers.
- Continuous oligomerization reaction mechanism was postulated by ReaxFF simulation.
- The monomer is easy to polymerize to form multimers at higher concentration.

ARTICLE INFO

Keywords:
Polymerization
Aluminate
Organic alkali
Initial nucleation stage
ReaxFF simulation

ABSTRACT

The reaction mechanism in the initial nucleation stages of organic alkali aluminate solution was obtained through reactive force field simulation. It was found that the hydrocarbon groups dissociated from tetramethylammonium cations ($TMAH^+$) acted as bridge in the process of aluminate polymerization. The monomer is easier to polymerize at higher concentration and $TMHA^+$ ions can promote the conversion of monomer. Moreover, the hydrocarbon group bonded $Al(OH)_4^-$ absorbs another $Al(OH)_4^-$ to form dimers and sequentially trimers, tetramers and higher polymerized aluminate ions. The elucidation of prenucleation species facilitates investigations of stability of aluminate solution and further guide the regulation of material morphology and crystal structure.

1. Introduction

The special crystal structure of Al_2O_3 with excellent mechanical and chemical performance has been widely used in many fields [1,2]. However, the manufacture of these highly qualified Al_2O_3 lacks instructive structural design and methods such as spherical alumina for lithium ion batteries membranes [3,4] and ternary cathode materials [5,6]. Structure regulation during the nucleation is the basis of designing new functional materials. In the industrial processing and preparation of Al_2O_3, it is important to clarify the pre-nucleation species and microscopic mechanism for subsequent regulation of morphology and structure [7]. However, the microscopic process is highly complicated, and the initial nucleation mechanisms of Al_2O_3 are far from being clear [8]. In recent years, multistep [9] or two-step [10] nucleation mechanisms of different crystal structures have been put forward. Gebauer [11], Quigley [12], Thanh [13] et al verified that prenucleation clusters intermediates in multistep nucleation determined the final crystal structure especially nucleation from solutions. Therefore, the intermediate structure and the reaction mechanism in the initial nucleation stage of aluminate solution were discussed in this study based on two step and multi-step nucleation theory.

Previous investigations focused on discrete aluminates intermediate structures existed in the caustic solution. It was hypothesized that most of these structures were isomers or molecules with similar composition. Generally, these structures differ from each other for only a few hydrogen atoms or water molecules. And then the most probable structure present in the solution was considered to be the ions of the most stable or of maximum reaction enthalpy. Based on ab initio quantum mechanical calculation and transition state theory, Chen [14] et al. put forward that the growth unit $[Al_6(OH)_{22}(H_2O)_2]^{4-}$ can be generated

* Corresponding author at: Key Laboratory of Green Process and Engineering, National Engineering Laboratory for Hydrometallurgical Cleaner Production Technology, Institute of Process Engineering, Chinese Academy of Sciences, Beijing 100190, PR China.
E-mail address: zwang@ipe.ac.cn (Z. Wang).

https://doi.org/10.1016/j.cplett.2019.136979
Received 11 October 2019; Received in revised form 15 November 2019; Accepted 21 November 2019
Available online 22 November 2019

due to transformation of aluminates coordination, and growth unit was proved to grow into critical nucleation point. The alternative means is by comparing vibrational spectrum such as UV–Vis, IR and Raman spectrum with theoretical simulation by different methods and basis sets. Liu [15] et al. concluded that 6AlO-OH and $[(OH)_2\text{-}Al\text{-}O_2\text{-}Al\text{-}(OH)_2]^{2-}$ were the intermediate structure by combining experimental UV–Vis and Raman measurements and density functional theory simulation. Chen [16] et al found that the maximum concentration of $Al(OH)_4^-$ occurs in low caustic solutions, but $Al(OH)_6^{3-}$ appear in high caustic solution by combining spectroscopy measurements and MD simulation.

Based on these discrete aluminates intermediate structures, merely partial polymerization process of aluminates were put forward or the transition pathways were proposed based on many assumptions. However, some results proved unreliable. Many structures have similar chemical and physical properties, and some can interconvert by small energy compensation. It is difficult to determine the precise transformation mechanism. Pouvreau [7] revealed that the μ-oxo $Al_2O(OH)_6^{2-}$ and di-μ-hydroxo $Al_2(OH)_8^{2-}$ were energetically separated by 2 kcal/mol in pure water but the stability of each can be reversed by ion pairing expected in saturated salt solution. However, challenges still remain to be elucidated clearly such as how the monomer evolves in the initial nucleation process.

Researchers have studied the evolving pathway of alumina monomer through various experimental monitoring methods, such as UV–Vis [15] dynamic light scattering [17] (DLS), muti-angle laser light scattering [18] (MALLS), TEM and X-ray diffraction [19]. Although the experimental detection techniques were intuitive and reliable, it was difficult to capture the fine structure changes between the microscopic and macroscopic scales in the initial nucleation stage, and there is no complete and clear understanding the structure of aluminate multimers. However, the accuracy and reliability of simulations are widely recognized with advanced computation methods and hardware advancement [20,21].

The reaction mechanism was explored in various systems especially in the initial nucleation stage by different computational simulation methods such as atomistic molecular dynamics simulation [22], Car-Parrinello molecular dynamics [23], metadynamics [24] and Density Functional Theory [25] (DFT). Therefore, computational simulation has become an indispensable method in investigating the initial nucleation process. Gale [25] et al. found that intermediate of hydroxyl bridged $(OH)_3Al(OH)_2Al(OH)_3^{2-}$ occured in high concentration sodium aluminate using ab initio methods at MP2 and B3LYP level. Watling [26] et al. concluded that aluminates formed clusters as a function of time and these clusters were stabilized by sodium ions. However, only some aluminate intermediate structures were put forward and the experimental vibrational spectra were in accordance with simulated spectra. The exact interaction among monomeric aluminates and reaction mechanism during the initial nucleation stages still remains obscure.

In order to understand the microscopic reaction mechanism in actual initial nucleation process of aluminate solution unambiguously, the reactive force field (ReaxFF) developed by van Duin [27] et al. provides an alternative approach. ReaxFF has been developed and widely used in various researches. It was applied to explore the combustion reaction path of hydrocarbon oxidation [28], thermal decomposition of cyclic-$[CH_2N(NO_2)]_3$ [29], hydrogenation reaction of zeolite [30], silicon and silicon oxide systems [31], and Al-water reaction [32] et al. Therefore, it is possible that the reaction force field can be used to study the reaction mechanism of initial nucleation stage of aluminate system.

All above analyses of alumina intermediate structures were carried out in caustic aluminate solution (NaOH). Wang [33] et al. substitute organic alkali for traditional caustic, and they proved that tetramethylammonium aluminate solution system can regulate the metastable zone width (MSZW) more easily than the sodium aluminate solution system by the Focused Beam Reflectance Measurement (FBRM) online real-time testing equipment. Tetramethylammonium aluminate aqueous was verified to be an excellent medium to control and explore the decomposition process of aluminates because of the better stability of the solution and more mild transformation process [34,35]. The mechanism analyzed by Wang [35] demonstrated that the dissociation equilibrium of choline hydroxide (pK_b = 1.3) restrict the complete dissociation of choline hydroxide in the initial Al-H_2O reaction stage and accelerate the regeneration of OH^- in the latter aluminates decomposition stage. The equilibrium between alkali depletion and regenerate make the system more moderate compared with NaOH (pK_b = 0.2). Compared with dissolution of gibbsite in NaOH solution, Shi [36] verified that the equilibrium solubility in choline is significantly lower, which was caused by the higher molecular weight of choline and more free water molecules in NaOH solution. The tetramethylammonium aluminate was selected considering various advantages of it. Therefore, how various ions interact with each other and what role does the cation play during the oligomerization were also discussed while discussing the intermediate structure and reaction mechanism.

In summary, we focus on the initial nucleation stage and use the ReaxFF calculation method to investigate the multimeric structure of the tetramethylammonium aluminate solution and its reaction mechanism. At the same time, the function of organic alkali aluminate solution system on aluminate polymer formation was explored. All of these results contribute to the prediction of transition structures or final crystal morphology in subsequent stages of nucleation.

2. Computational methods and models

All the molecules were placed in a three dimensional cube with edge of 18 Å. Three types of models with different chemical components were constructed for the simulations:

Model A: 21 aluminate anions ($Al(OH)_4^-$), 15 hydroxide ions (OH^-), 36 organic alkali cations ($TMAH^+$: $NC_4H_{12}^+$), and 486 water molecules (H_2O).
Model B: 21 $Al(OH)_4^-$, 15 OH^-, and 486 H_2O.
Model C: 5 $Al(OH)_4^-$, 1 OH^-, 6 $TMAH^+$, and 10 H_2O.

The aluminate concentration in Model A is 5.98 mol L^{-1} (high concentration), and alkali concentration is 10.27 mol L^{-1}. Model A was arranged to study the reaction mechanism in the initial nucleation stages of the organic alkali aluminate system; Model B was designed to investigate the microscopic effects of organic base cations on the polymerization process. Hence non-reactive positive charge was added to the Model B to achieve charge balance; low concentration of Al $(OH)_4^-$ (1.4 mol L^{-1}) and TMAH (1.7 mol L^{-1}) in Model C was used to investigate the difference of microscopic mechanism at different concentrations.

The canonical ensemble (NVT) of all three models was implemented using Lammps [37] that contain the ReaxFF package. The initial structure was constructed using Packmol [38] software and converted to the data files required by Lammps using VMD [39] software, and the initial atomic charge was assigned using the classical force field. The input files include three major parts: energy minimization, system equilibration, and NVT-MD simulation. The total duration of the simulation is 1 ns and the time step of integration is 0.1 fs. Minimization was performed at 0 K to ensure that no overlap occurred in the initial configuration. The NVT ensemble was used during the equilibration and the total simulation time for this period is 20 ps. It is worth noting that there is no reaction against the system when the equilibrium is carried out, and the ReaxFF parameters were modified to avoid the reaction in this stage [40]. The ReaxFF molecular dynamics simulation was carried out in the final stage, and the simulation temperature was set as 363 K which was the temperature of our previous work [33,35]. The Berendsen thermoset with a damping constant of 10 fs was used to control temperature. The perform charge equilibration (QEq) method

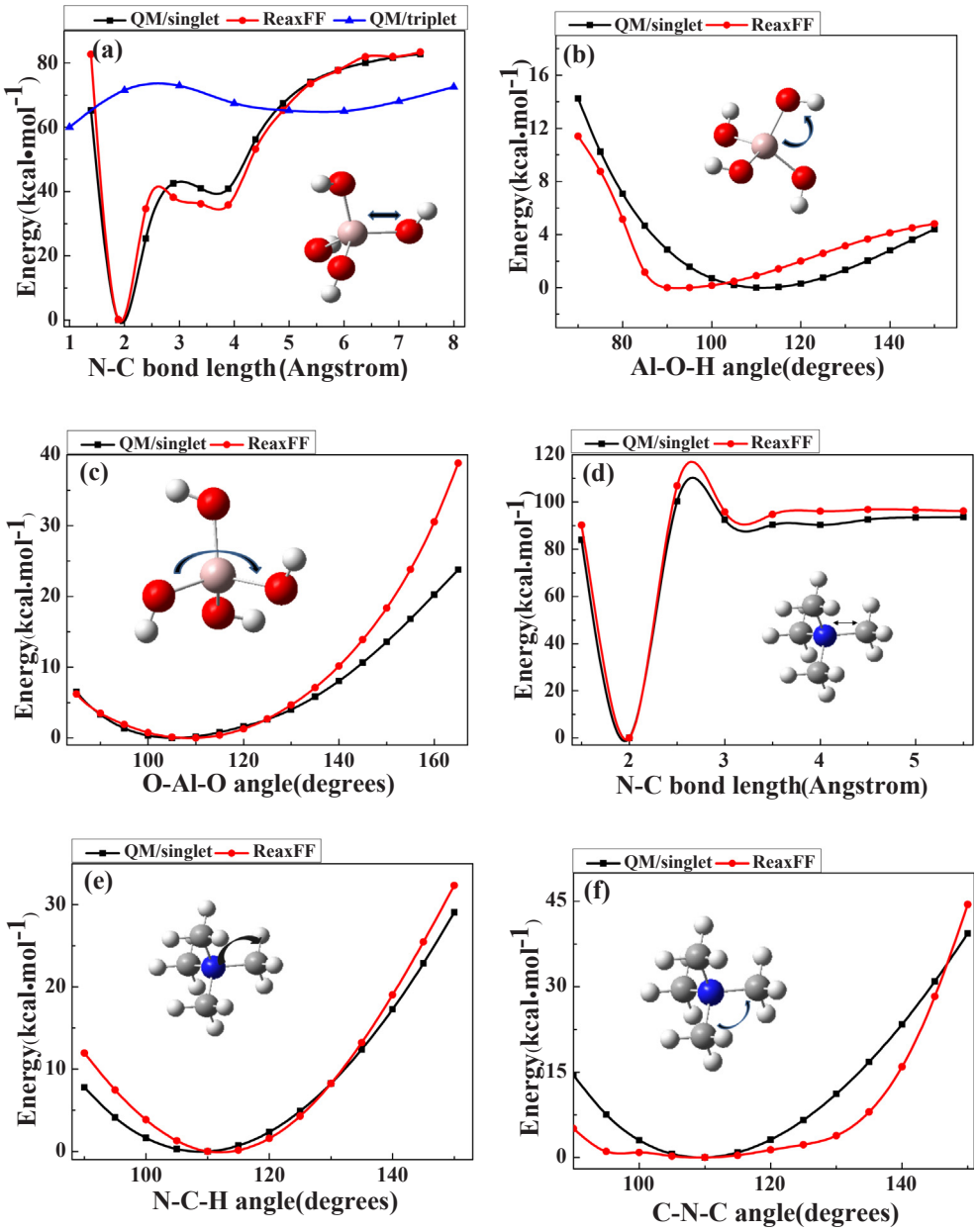

Fig. 1. The energy difference between QM and ReaxFF of the typical bonds and angles in $Al(OH)_4^-$ and $TMAH^+$ molecules. (a) bond stretching energy of Al—O in $Al(OH)_4^-$, (b) energy of Al—O—H angle bending in $Al(OH)_4^-$, (c) O—Al—O angle bending energy in $Al(OH)_4^-$, (d) bond stretching energy of N—C in $TMAH^+$, (e) N—C—H angle bending energy in $TMAH^+$, and (f) C—N—C angle bending energy in $TMAH^+$. Element colors are red for oxygen, dark pink for aluminum, light white for hydrogen, dark blue for nitrogen and gray for carbon atom.

[41] was used to calculate the charge on each atom which lead to energy minimization of the system.

The parameters have been trained for the interactions relevant to the simulations. The ReaxFF force field parameters for H, C, O, N, and Al were derived from the data developed by Psofogiannakis [30] et al. on the basis of van Duin's work [27]. The parameters relating to Al were derived from the calculation and optimization of $Al(OH)_3$ using the original ReaxFF parameters. Hence, the parameters do contain the full set of interactions that observed in the simulation. The results of the bond stretching and angle bending energy calculated by ReaxFF calculation were compared with DFT calculation to ensure all the parameters used were applicable to the above system. The DFT calculations of $Al(OH)_4^-$ and $TMAH^+$ species were performed using Gaussian 09 [42] package at DFT/B3LYP level with 6–31 g + (d, p) basis set.

3. Results and discussion

3.1. Applicability

The molecules used for parameterization are given in Fig. 1 and the verification of this method is developed by comparisons between the energy differences between the force field and QM values of the typical bonds and angle in clusters [43]. The figure show comparisons between energy results of Al—O bond and N—C bond stretching, Al—O—H angle, O—Al—O angle, N—C—H angle and C—N—C angle bending by force field and DFT calculation. Two electronic states of singlet and triplet were conducted when calculating the Al—O bond stretching energy with DFT calculation. The Al—O dissociation energy of singlet state is smaller than the energy of triplet state at short range as seen from Fig. 1a. Conversely, the energy of singlet is higher than that of triplet when the distance larger than 1.5 Å. Obviously, the results of QM with singlet state and ReaxFF calculations are in good agreement. When the angles of Al—O—H, O—Al—O, N—C—H and C—N—C are at degrees of about 110, the results of ReaxFF and DFT completely overlap, and the

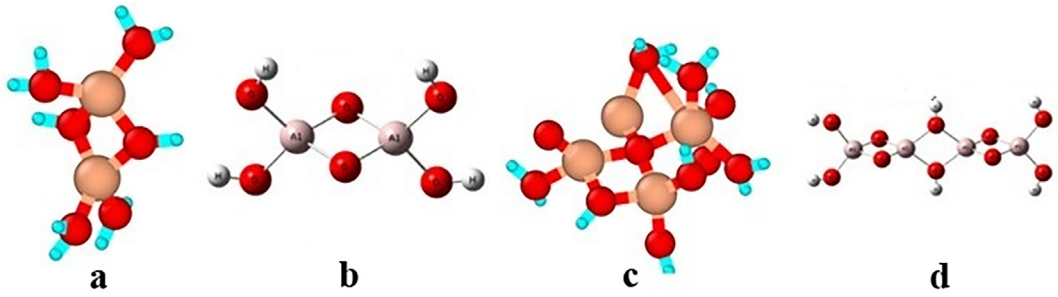

Fig. 2. Dimer and tetramer aluminate structure. (a) dimer aluminate simulated by ReaxFF, (b) $Al_2O_6H_4^{2-}$ dimer in ref 15. (c) tetramer aluminate simulated by ReaxFF, and (d) $Al_4O_{10}H_6^{2-}$ tetramer in ref 15. Element colors are red for oxygen, dark pink for aluminum and light blue for hydrogen atom.

deviation is minimum. In general, the energy error from different simulation method of $Al(OH)_4^-$ is 4 kJ mol^{-1} and the error of $TMAH^+$ is 6 kJ mol^{-1}. The comparisons show that the force field represents the energy curves well near the minimum, but the deviations become larger with increased angles. It shows that the results calculated by force field are in good agreement with DFT. Hence, ReaxFF was employed instead of QM to calculate $Al(OH)_4^-$ and organic alkali ions for the purpose of simplification.

In addition, the simulation results of sodium aluminate solution system calculated with ReaxFF force field are consistent with the analysis of Liu [15] et al. Liu concluded that aluminate dimer (Fig. 2b) and tetramer (Fig. 2d) appeared during the decomposition of sodium aluminate solution by DFT calculation. It is apparent that aluminum atoms are linked by oxygen atoms in these structures as shown in Fig. 2 and the structures obtained by ReaxFF simulation are consistent with the structures of $Al_2O_6H_4^{2-}$ and $Al_4O_{10}H_6^{2-}$ inferred by DFT calculation [15]. These force fields parameters are proper for describing the chemical interactions in the organic aluminate system. Consequently, the force field can be transferred to the organic aluminate system. It is inferred that ReaxFF is a reliable method to simulate aluminate solution.

3.2. Model A

Fig. 3 displays the population of the main species as a function of time obtained in 1 ns simulation which was conducted at 370 K. Partial water molecules decompose into hydroxyl ion and proton rapidly while some absorb hydroxyl ions presented in the system to form charged hydrogen-oxygen molecules. It is named H_xO_y. The number of H_2O and H_xO_y were counted together. Water mainly decomposed before 220 ps, the remained undecomposed water molecules absorbed hydroxyl groups from 220 to 250 ps. The $TMAH^+$ decomposed into nitrogen-containing hydrocarbon small molecules rapidly in the initial stage, and the total number maintained at around 120. Some $Al(OH)_4^-$ ions combined with free hydroxide ions and transformed into AlO_mH_n (m between 1 and 5, n between 5 and 10). The remained $Al(OH)_4^-$ interacted with hydrocarbon molecules and carbon-containing aluminate molecules AlO_mH_n-C_xH_y (m between 1 and 5, n between 4 and 9, x between 1 and 2, y between 2 and 6) were formed. The number of AlO_mH_n and AlO_mH_n-C_xH_y increased and decreased respectively. The total number remained at 18 but it was less than the initial number of aluminates. It indicates that the monomer aluminate can convert into other forms of polymerized aluminate as depicted in Fig. 2b.

Dimerized aluminates $Al_2O_mH_n$ (m between 3 and 7, n between 6 and 12) formed at 15 ps and hydrocarbon-containing dimers formed afterwards in spite of its instability. Similar with dimerized aluminates, hydrocarbon contained $Al_aO_mH_n$-(N)C_xH_y (a = 2, 3, 4) and unstable hydrocarbon free $Al_aO_mH_n$ are generated successively as illustrated in Fig. 3b. As the number of molecules of $Al_3O_mH_n$ (m between 4 and 10, n between 9 and 21) increased, the number of molecules of $Al_2O_mH_n$-(N)C_xH_y (m between 3 and 7, n between 6 and 12, x between 1 and 3, y between 2 and 4) decreased simultaneously. Hence, the generation of $Al_3O_mH_n$ is formed at the dispense of consumption of $Al_2O_mH_n$-(N)C_xH_y。 Moreover, the number of trimers and dimers with hydrocarbon groups reduces simultaneously while the number of tetramers increases, indicating that the formation of tetramer aluminate is derived not only from $Al_3O_mH_n$-(N)C_xH_y (m between 4 and 10, n between 9 and 21, x between 1 and 4, y between 2 and 9) but also from $Al_2O_mH_n$-(N)C_xH_y. All above prove that dimers, trimmers, tetramers and highly polyaluminate ions are formed by absorbing $Al(OH)_4^-$ stepwise from hydrocarbon group bonded $Al(OH)_4^-$. This suggests that the hydrocarbon groups act as the bridge in the process of aluminate

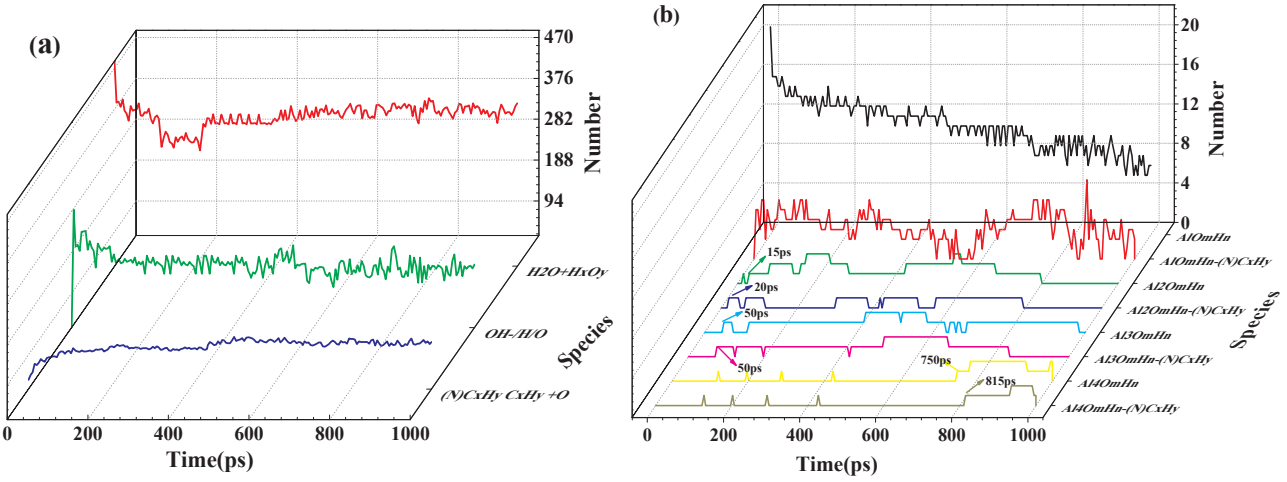

Fig. 3. Species distributions as function of simulation time (0–1 ns) in Model A. The simulation is carried out at 370 K.

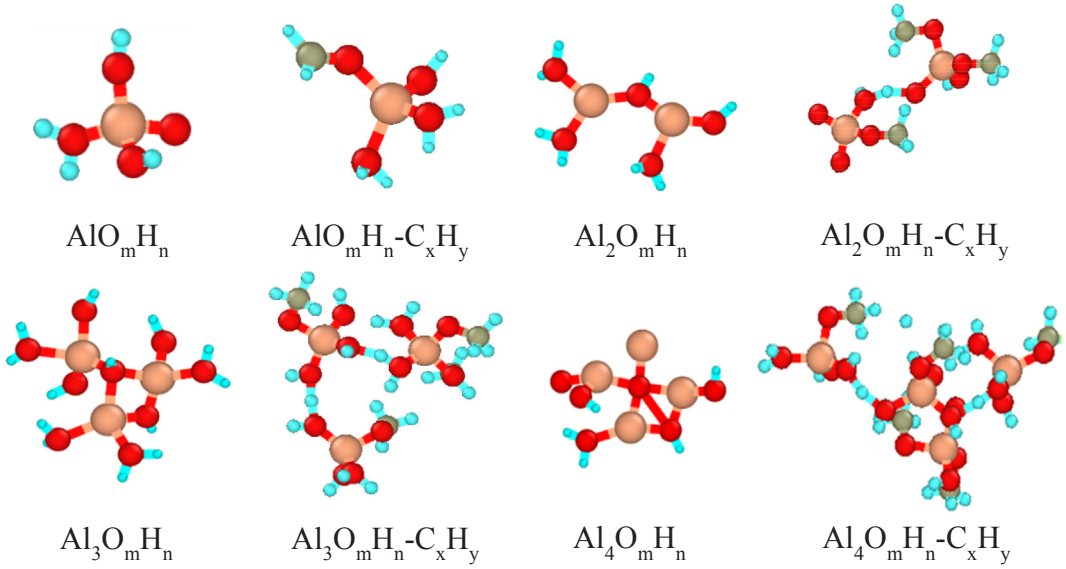

Fig. 4. Hydrocarbon and hydrocarbon-free polymerized aluminate configurations captured during the simulation.

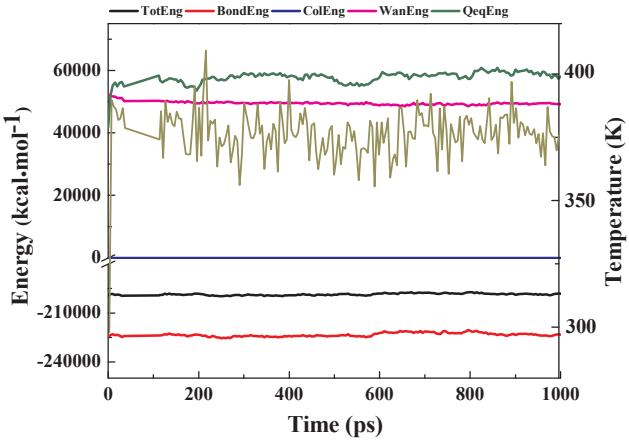

Fig. 5. The energy and temperature fluctuation with time evolution.

polymerization. Fig. 4 shows the aluminate monomer and polymer configurations captured during the simulation of the system.

In order to further illuminate how the monomers convert to multimers and the final configuration of the polymer. The energy curves were investigated. As shown in Fig. 5, the total energy stabilized at $-200{,}000$ kJ mol^{-1}, and the bond energy stabilized at $-225{,}000$ kJ mol^{-1}. The sum of van der Waals and charge energy is 5000 kJ mol^{-1}, and the Coulomb force fluctuated at -50 kJ mol^{-1}. Therefore, there is always an exchange of charge and electrostatic force in the system, indicating the conversion among aluminate structures. Trimer sequentially transfers to the tetramer from the captured video animation (see S.1 in details). Most aluminates converted to tetramer after 750 ps. The aluminum atoms bonded with two oxygen atoms and the two oxygen atoms also bonded with each other which are similar to the bonding way of gibbsite as shown in Fig. 6. It can be seen that at given concentration and temperature of 370 K, in the initial pre-nucleation stage aluminate monomer converted to dimer aluminate and then transformed into trimer, tetramer and higher poly-aluminate during which hydrocarbon-containing aluminate monomers and multimers served as intermediates. It can provide initial basic configuration for subsequent nucleation and growth phases.

In order to further illustrate the existence of polymerized aluminates, the radical distribution functions (RDFs) of the system are analyzed. Fig. 7a shows the RDFs of aluminium to aluminium, oxygen and hydrogen. The maximum peak of Al—O and Al—H located at 2 Å and 2.5 Å respectively, which were similar with the intramolecular distance of Al—O and Al—H in $Al(OH)_4^-$ molecules (Al—O at 1.7 Å and Al-H at 2.2 Å in $Al(OH)_4^-$). The first-neighbour Al—Al peak in aluminate was observed at 2.7 Å, which was well consistent with interatomic of Al—Al distance in dimer aluminate (Al—Al at 2.5 Å in $Al_2O_mH_n$) which was shown in Fig. 4. So the RDFs distribution characteristics of Al—Al also indicated the formation of stable polymerized aluminate. In addition, a secondary peak of Al—Al appeared at 3.3 Å, a gentle peak at 5.6 Å, a small peak at 4.5 Å for Al—O, and a smooth peak at 5.8 Å for Al—H. It also implied higher oligomerized aluminum was formed. Fig. 7.b shows the RDFs of Al—N and Al—C. Although Al—N and Al—C have peaks at different distances, the intensities of peaks are negligible, indicating that the probabilities of formation of Al—N and Al—C ion pair are

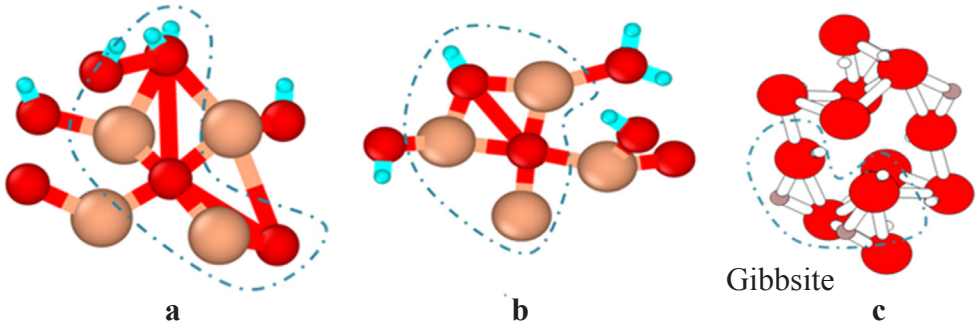

Fig. 6. Structures of (a, b) tetramers aluminate captured during Model A, and (c) Gibbsite crystal [44]. Where H atom is white, other atoms same as figure a.

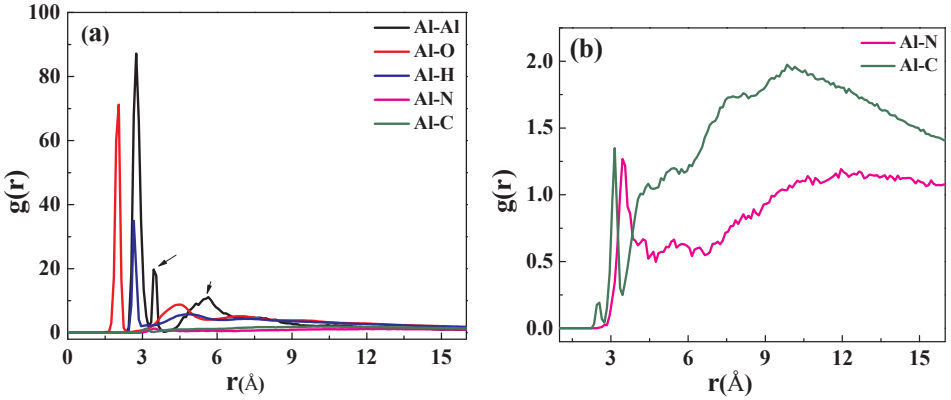

Fig. 7. RDFs in Model A. (a) for Al—Al, Al—O, Al—H, Al—N and Al—C and (b) for Al—N and Al—C.

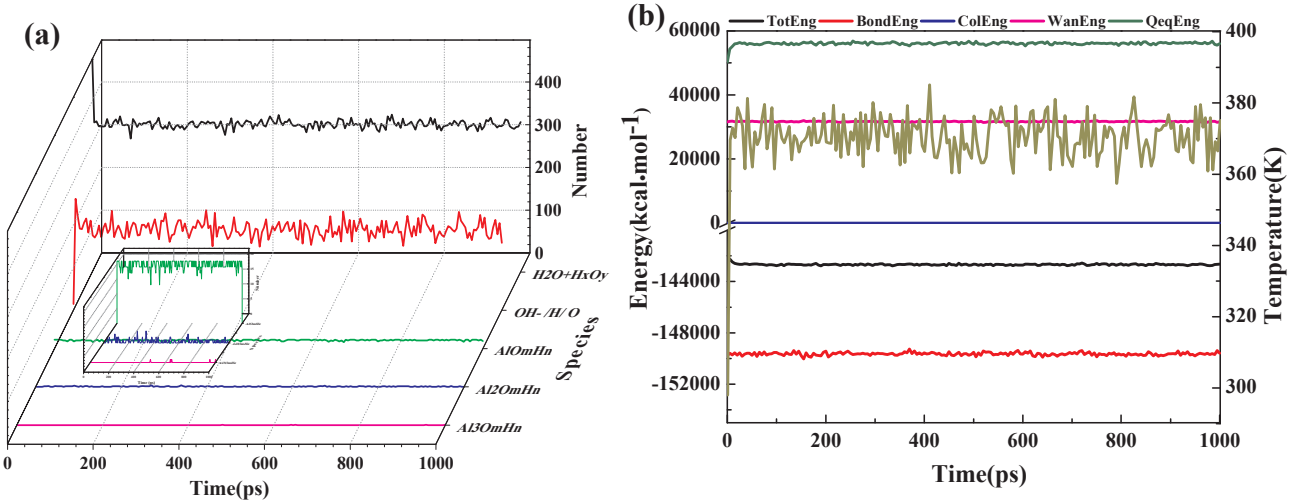

Fig. 8. (a) Species distributions and (b) the change of energy and temperature in Model B.

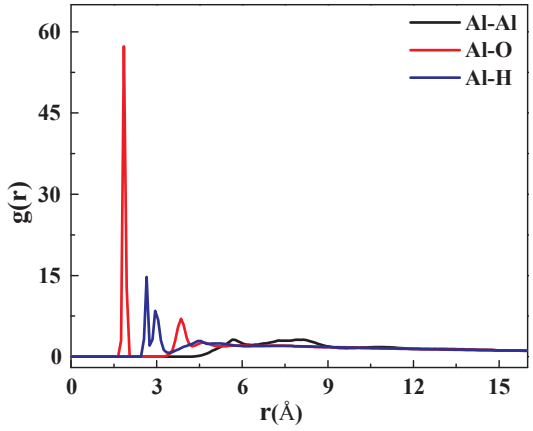

Fig. 9. RDFs for the Al—Al, Al—O, and Al—H.

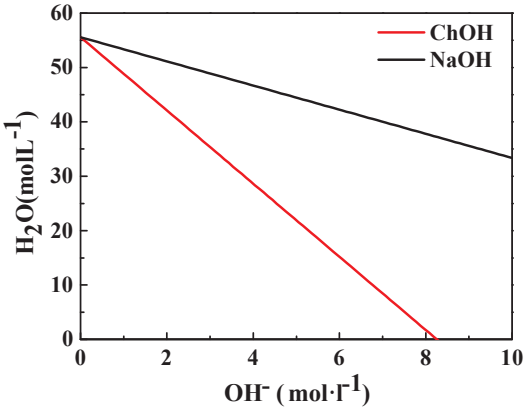

Fig. 10. The concentration of water molecules in alkaline solution as a function of OH^- concentration [36].

extremely low, and they are unstable even if they exist. It also suggests that the hydrocarbon groups acts as bridge in the process of aluminate polymerization.

3.3. Model B

Above analysis showed the presence of hydrocarbon-containing polymer aluminate, and there is no doubt that hydrocarbons are derived from $TMAH^+$ cations. Therefore, Model B was designed to investigate the microscopic effects of organic base cation in the initial stages, and non-reactive positive charge was added to the box instead of $TMAH^+$ during the calculation to achieve charge balance. Fig. 8a showed the population of all molecule species. The variation tendency of water molecules and hydroxide was the same as that in Model A. The monomeric aluminate molecules were stable and the number fluctuated around 20. In addition to original monomeric aluminate, a few unstable dimer and trimer aluminates were captured. Compared to the stable trimers and tetramers aluminates emerged in Model A, Model B clearly did not have the ability to generate higher polymerized multimers, so it consumed less OH^- and H_xO_y ions, since the number of H_xO_y and OH^-

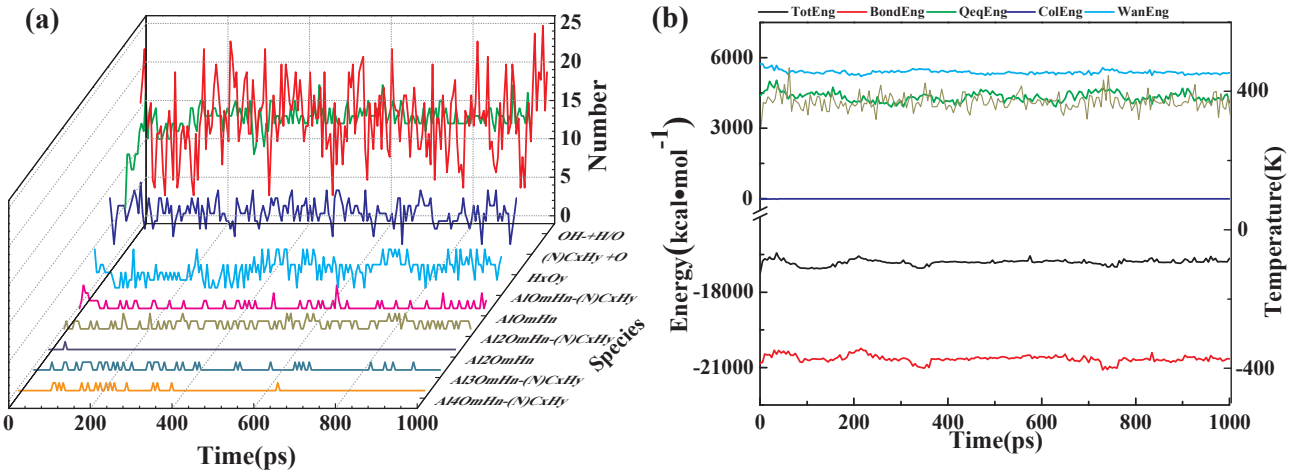

Fig. 11. (a) Species distributions and (b) the fluctuation of energy and temperature as function of simulation time (0–1 ns) in Model C.

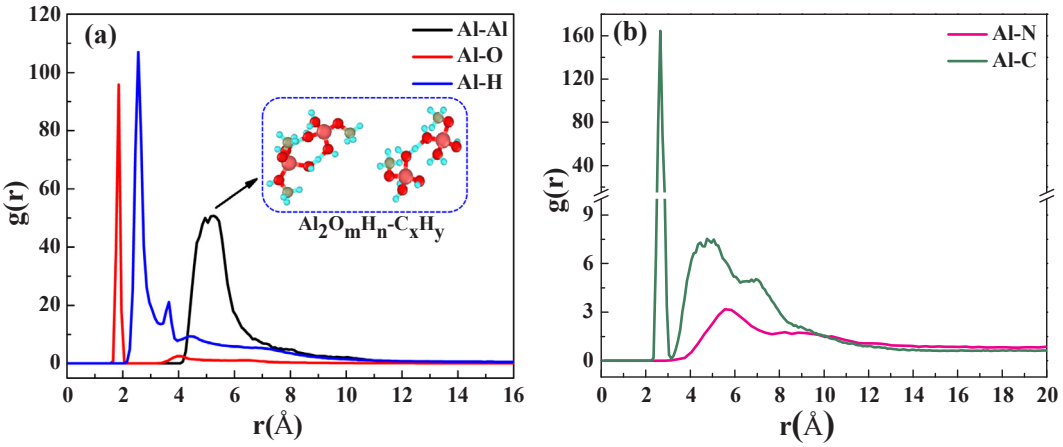

Fig. 12. RDFs for the Al—Al, Al—O, Al—H, Al—C and Al—N.

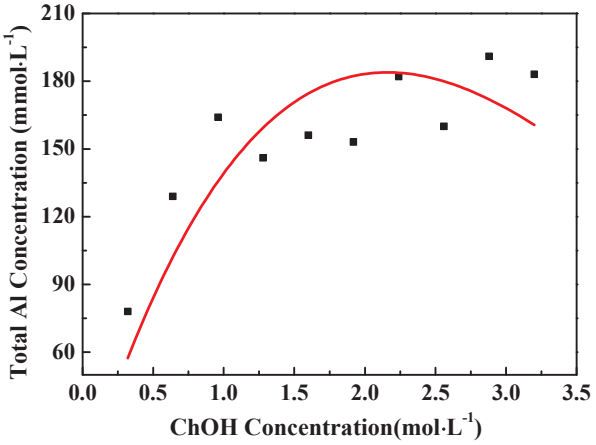

Fig. 13. Gibbsite equilibrium solubility in choline at 90 °C [36].

was more than in Model A. In terms of energy variation (Fig. 8b), the energy fluctuation of total energy, bond energy and coulombic force were less than the energy of Model A, thus indicating that the polymerization reaction was more preferred in Model A.

The RDFs of aluminium to aluminium, oxygen and hydrogen were carried out to further discuss the existence of the multi-component aluminate in Model B. It can be seen from Fig. 9 that the peak of Al—Al was not obvious except a tiny peak at 5.8 Å. Therefore the formation probability of polymerized aluminate is extremely low. The maximum peak of Al—O lay at 1.9 Å and two minor peaks at 3.9 Å and 4.6 Å respectively. At the same time, Al—H's major peak aroused at 2.7 Å, and a secondary peak at 3.0 Å. It was illustrated that merely stable monomeric AlO_mH_n molecules existed in the system, which was consistent with the results of Fig. 8a. On the basis of the two models with or without $TMAH^+$ cation, we conclude that the hydrocarbon group dissociated from $TMAH^+$ acts as bridge in the process of aluminate evolution. The organic base cation promote the conversion from monomer to polymeric multimers. At the same time, it explained the slow crystallization in the caustic alkali aluminate system. It is consistent with experimental results of solubility, as shown in Fig. 10, the data obtained by Shi[36] showed that the concentration of water in organic alkali solution decreased more rapid than in NaOH solution. The higher molecular weight of basic molecular is, the more free water molecules in solution. Hence, the equilibrium solubility of gibbsite in choline is significantly lower. In other word, the promotion of crystallization is more evident in organic base.

3.4. Model C

Model C was implemented to study the microscopic reaction mechanism at low concentration. Fig. 11a collected the number of major species and temperature curves during the 1 ns simulation. The molecular species in this model is apparently less compared with Model A. But the number of carbon-containing monomers was more than Model A. The total energy of Model C is basically stable and the fluctuation is

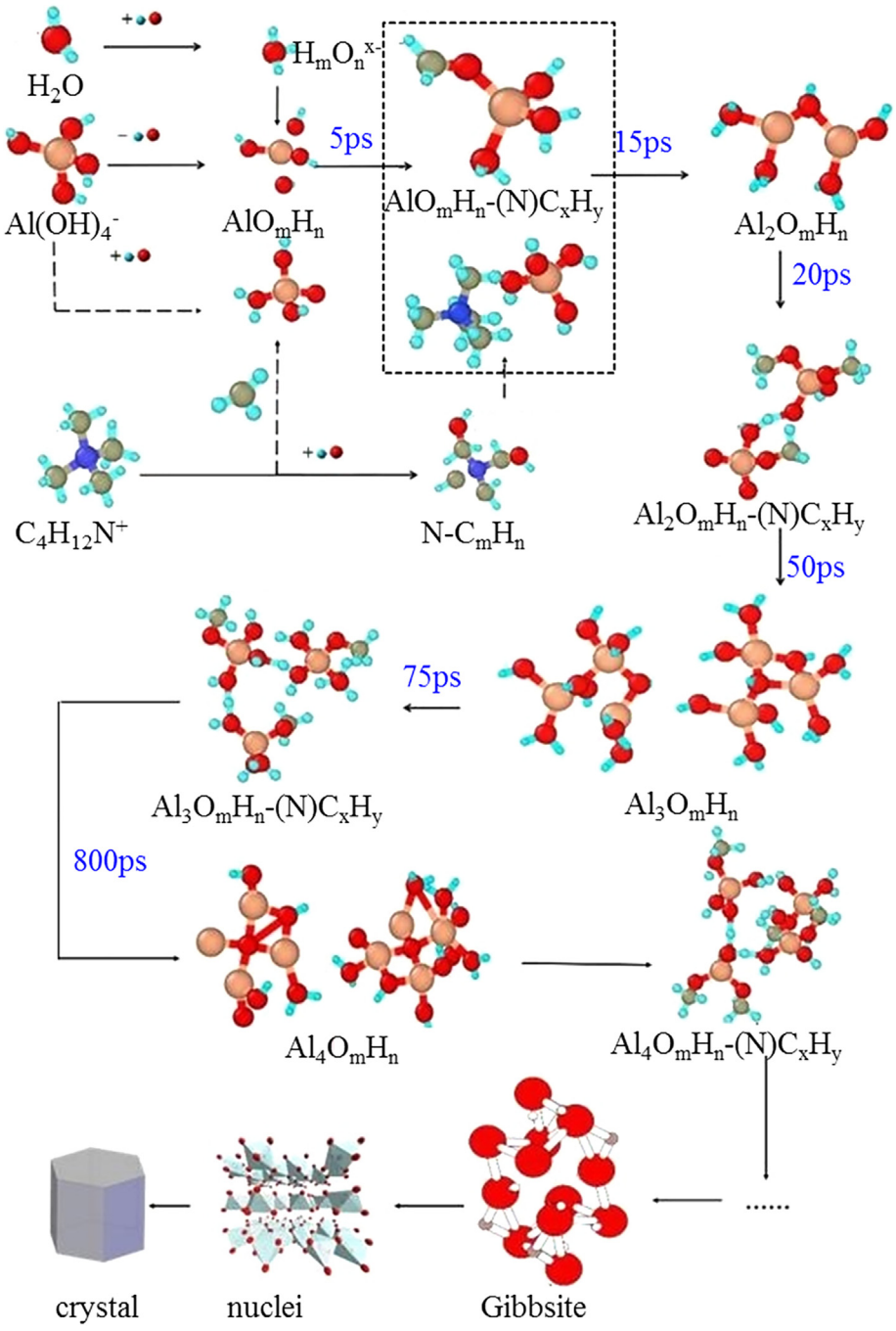

Fig. 14. Reaction mechanism in $TMAH^{+}$ aluminate solution.

smaller than Model A as shown in Fig. 11b, it indicated that the reaction rates was more slow in Model C. As depicted in Fig. 11a, the hydrocarbon-containing monomers exist stably, but the hydrocarbon-containing aluminate dimers and other polymer aluminates are unstable. The conclusion can be drawn that aluminate polymer cannot form at low concentration.

Fig. 12 showed RDFs of aluminum and other elements in the system. The largest peak of Al-Al located at 4.9 Å and 5.3 Å, which was responsible for the distance between Al and Al in hydrocarbon containing aluminate dimer (shown in the inset of Fig. 12). The unimodal peak at 1.84 Å of Al—O represent the existence of monomeric $Al(OH)_4^-$ in the system. Therefore, it is impossible to form naked aluminates and hydrocarbon groups contained aluminates higher than dimer because of its low stability. The detailed dynamic conversion process is displayed in movie S.2. Results of Model C implied that carbon-containing Al $(OH)_4^-$ was easily formed at low concentration, and higher polymerized aluminates were unable to exist. At the same time, this microscopic feature can also be explained from macroscopic phenomena. The fitted solubility curve of gibbsite at different choline concentrations was shown in Fig. 13. The solubility of gibbsite began to decrease when the alkali concentration exceed 2.25 mol L^{-1}. Based on this condition, the solubility of gibbsite corresponding to model A is significantly lower than that of model C. Therefore, it can promote the formation of higher polymerized aluminate and it is easier to further crystallize under the condition of model A.

3.5. Reaction mechanism

By analyzing and comparing the results of the three models, the bridge effect of $TMAH^+$ on the oligomerization of aluminate monomer was obtained. At the same time, the microscopic reaction mechanism of the polymerization process of organic alkali aluminate also became clear as shown in Fig. 14. The hydrocarbon-containing monomer aluminate is formed first through combining with $TMAH^+$ cation. But the hydrocarbon group is easy to dissociate from hydrocarbon-containing monomer aluminate due to the instability. Two hydrocarbon groups free monomeric aluminate combine with each other and subsequently a dimer aluminate is formed. Taking electronegativity into account, it is easy for dimer aluminate ions absorb free hydrocarbon ions to form hydrocarbon-containing dimer aluminates, followed by trimers, tetramers and higher polymerized aluminates. Considering that all simulations were conducted on 1 ns time scale and limited molecules in the system, higher polymerized aluminate didn't emerge. However, the polymerized aluminate is likely to serve as the precursor of gibbsite since the structure of the tetramer aluminate is similar to the crystal structure of gibbsite. According to this microscopic polymerization mechanism, the gibbsite crystal may be obtained at subsequent nucleation stage. Therefore, all this help to regulate the mesoscale intermediate structures or prenucleation species at the microscopic level in initial nucleation stages.

4. Conclusions

(1) The reactive force field parameters were verified to be adequate for the investigation of structural and reaction mechanism of tetramethylammonium aluminate solution. Dimers, trimmers, tetramers and highly polyaluminate ions were formed by absorbing $Al(OH)_4^-$ stepwise from hydrocarbon group bonded $Al(OH)_4^-$. It helps to regulate the mesoscale intermediate structures at the microscopic level in initial nucleation stages, and guide the subsequent polymerization process.
(2) The hydrocarbon-containing aluminate is transitional intermediate structure for the conversion process of monomers to polyaluminate by comparing two models with or without organic base cation. In other words, the $TMAH^+$ cation serves as a bridge in the process of aluminate polymerizations and it promotes the crystallization of aluminate solution.
(3) At low organic alkali aluminate concentration of 1.4 mol L^{-1}, oligomeric aluminates higher than dimer can hardly formed, indicating that the aluminate monomer is difficult to polymerize in the initial stage of nucleation at low concentration.

5. Contributions

Jianwei Guo, Shuangyi Liu and Zhi Wang designed the simulations and experiments. Jianwei Guo and Shuangyi Liu conducted all the simulations and experiments. The data analysis was performed by Shuangyi Liu and Jianwei Guo. Zhi Wang, Jianwei Cao and Dong Wang provided scientific advice on data analysis. Shuangyi Liu and Jianwei Guo prepared the figures and drafted the manuscript. All the authors discussed, reviewed, and commented on the manuscript.

Declaration of Competing Interest

The authors declare that they have no known competing financial interests or personal relationships that could have appeared to influence the work reported in this paper.

Acknowledgements

This work was partially funded by the National Key R&D Program of China (2018YFC1901801) and the National Natural Science Foundation of China (51974286).

Appendix A. Supplementary material

Supplementary data to this article can be found online at https://doi.org/10.1016/j.cplett.2019.136979.

References

[1] T. Guo, X. Nie, J. Du, J. Li, Chem. Eng. J. 361 (2019) 1345.
[2] V.K. Das, R.R. Devi, P.K. Raul, A.J. Thakur, Green. Chem. 14 (2012) 847.
[3] Q. Li, L. Zhang, S. Wei, Y. Zhang, R. Sun, T. Zhou, W. Bu, Q. Yao, Z. Jiang, H. Chen, Ceram. Int. 44 (2018) 11374.
[4] J. Kong, B. Chao, T. Wang, Y. Yan, Powder Technol. 229 (2012) 7.
[5] W. Xiang, W.Y. Liu, J. Zhang, S. Wang, T.T. Zhang, K. Yin, X. Peng, Y.C. Jiang, K.H. Liu, X.D. Guo, J. Alloys. Compd. 775 (2019) 72.
[6] K.J. Park, M.J. Choi, F. Maglia, S.J. Kim, K.H. Kim, C.S. Yoon, Y.K. Sun, Adv. Energy. Mater. 8 (2018) 1703612.
[7] M. Pouvreau, M. Dembowski, S.B. Clark, J.G. Reynolds, K.M. Rosso, G.K. Schenter, C.I. Pearce, A.E. Clark, J. Phys. Chem. B 122 (2018) 7394.
[8] P. Sipos, J. Mol. Liq. 146 (2009) 1–14.
[9] N.D. Loh, S. Sen, M. Bosman, S.F. Tan, J. Zhong, C.A. Nijhuis, P. Kral, P. Matsudaira, U. Mirsaidov, Nat. Chem. 9 (2017) 77.
[10] P.G. Vekilov, Nanoscale 2 (2010) 2346.
[11] D. Gebauer, M. Kellermeier, J.D. Gale, L. Bergstrom, H. Colfen, Chem. Soc. Rev. 43 (2014) 2348.
[12] D. Quigley, P.M. Rodger, J. Chem. Phys. 128 (2008) 221101.
[13] N.T. Thanh, N. Maclean, S. Mahiddine, Chem. Rev. 114 (2014) 7610.
[14] Q.Y. Chen, J. Li, Z.L. Yin, P.M. Zhang, T. Nonferr. Metal. Soc. 13 (2003) 649.
[15] W. Liu, Y.L. Huang, Z.L. Yin, Z.Y. Ding, J. Mol. Liq. 261 (2018) 115.
[16] Y. Chen, Q.M. Feng, K. Liu, Y.D. Chen, G.F. Zhang, Chem. Phys. Lett. 422 (2006) 406.
[17] D.R. Harris, R.I. Keir, C.A.T. Prestidge, J.C. Thomas, Colloid Surf. A 154 (1999) 343.
[18] D.S. Rossiter, P.D. Fawell, D. Ilievski, G.M. Parkinson, J. Cryst. Growth. 191 (1998) 525.
[19] J.S.C. Loh, A.M. Fogg, H.R. Watling, G.M. Parkinson, D. O'Hare, Phys. Chem. Chem. Phys. 2 (2000) 3597.
[20] S.J. Marrink, A.H. de Vries, A.E. Mark, J. Phys. Chem. B 108 (2004) 750.
[21] W.C. Swope, H.C. Andersen, P.H. Berens, K.R. Wilson, J. Chem. Phys. 76 (1982) 637.
[22] R. Demichelis, P. Raiteri, J.D. Gale, D. Quigley, D. Gebauer, Nat. Commun. 2 (2011) 590.
[23] J. Saukkoriipi, K. Laasonen, J. Chem. Theory Comput. 6 (2010) 993.
[24] D. Quigley, P.M. Rodger, C.L. Freeman, J.H. Harding, D.M. Duffy, J. Chem. Phys. 131 (2009) 094703.
[25] J.D. Gale, A.L. Rohl, H.R. Watling, G.M. Parkinson, J. Phys. Chem. B 102 (1998) 10372.
[26] H.R. Watling, S.D. Fleming, W. van Bronswijk, A.L. Rohl, J. Chem. Soc., Dalton Trans. (1998) 3911.
[27] A.C.T. van Duin, S. Dasgupta, F. Lorant, W.A. Goddard, J. Phys. Chem. A 105 (2001) 9396.
[28] K. Chenoweth, A.C.T. van Duin, W.A. Goddard, J. Phys. Chem. A 112 (2008) 1040.
[29] A. Strachan, E.M. Kober, A.C. van Duin, J. Oxgaard, W.A. Goddard, J. Chem. Phys. 122 (2005) 54502.
[30] G.M. Psofogiannakis, J.F. McCleerey, E. Jaramillo, A.C. van Duin, J. Phys. Chem. C 119 (2015) 6678.
[31] J.C. Fogarty, H.M. Aktulga, A.Y. Grama, A.C.T. van Duin, S.A. Pandit, J. Chem. Phys. 132 (2010) 174704.
[32] M.F. Russo, R. Li, M. Mench, A.C.T. van Duin, Int. J. Hydrogen Energy 36 (2011) 5828.
[33] H.Q. Wang, Z. Wang, L. Liu, X.Z. Gong, M.Y. Wang, Cryst. Growth Des 16 (2016) 1056.
[34] H.Q. Wang, Z. Wang, J.W. Guo, Z.H. Shi, X.Z. Gong, J.W. Cao, Cryst. Growth Des 17 (2016) 183.
[35] H.Q. Wang, Z. Wang, Z.H. Shi, X.Z. Gong, J.W. Cao, M.Y. Wang, Energy 131 (2017) 98.
[36] Z. H. Shi, Graduate thesis (2016) Guangxi Normal University.
[37] S. Plimpton, J. Comput. Phys. 117 (1995) 1.
[38] L. Martinez, R. Andrade, E.G. Birgin, J.M. Martinez, J. Comput. Chem. 30 (2009) 2157.
[39] W. Humphrey, A. Dalke, K. Schulten; 1996.
[40] K.D. Nielson, A.C.T. van Duin, J. Oxgaard, W.Q. Deng, W.A. Goddard, J. Phys. Chem. A 109 (2005) 493.
[41] A.K. Rappe, W.A. Goddard, J. Phys. Chem.-Us. 95 (1991) 3358.
[42] M.J. Frisch, et al., Gaussian 09, Gaussian Inc, Wallingford CT, 2016.
[43] C. Bai, L. Liu, H. Sun, J. Phys. Chem. C 116 (2012) 7029.
[44] K. Nikoofar, Y. Shahedi, F. Chenarboo, Mini-Rev. Org. Chem. 16 (2019) 102.